

Electrocatalytic performance of MoS₂ nanosheets grown on a carbon nanotubes/carbon cloth substrate for the hydrogen evolution reaction

J. L. Zhu^a, J. X. Zhang^a, J. Liu^c, Z. Liu^a, Y. D. He^a, A. X. Wei^{a,b,*}

^a*School of Material and Energy, Guangdong University of Technology, Guangzhou 510006, Guangdong, China*

^b*School of Information Science, Guangzhou Xinhua University, Dongguan 523133, Guangdong, China*

^c*School of Electrical Engineering, University of South China, Hengyang 421001, Hunan, China*

Two dimensional (2D) layered molybdenum sulfide (MoS₂) exhibit unique advantages as electrocatalyst for the hydrogen evolution reaction (HER). However, the low conductivity of MoS₂ itself still limit the overall HER rate. In this work, MoS₂ nanosheets grown on a carbon nanotubes (CNTs)/carbon cloth (CC) were used as a cathode electrode for HER under alkaline electrolysis. A MoS₂/CNTs/CC were prepared by a hydrothermal method using a precursor solution of sodium molybdate (Na₂MoO₄·2H₂O), thiourea (SC(NH₂)₂), oxalic acid (C₂H₂O₄·2H₂O) and deionized water. The oxalic acid is used as a reducing agent and its concentration plays a significant role in controlling the size and the HER performance of MoS₂ nanosheets. The MoS₂/CNTs/CC catalyst prepared with the oxalic acid concentration of 5.625 mM shows the optimal HER activity, exhibiting the overpotential of 134 mV at a current density of 10 mA cm⁻², Tafel plots of 45.7 mV dec⁻¹, electrochemical double layer capacitance of 123.9 mF cm⁻², electrochemical surface area of 3097.5 cm² and very high durability. The improved HER activity is attributed to the more exposed active sites for the smaller size MoS₂ nanosheets and improved conductivity of MoS₂ nanosheets by CNTs.

(Received April 24, 2022; Accepted July 20, 2022)

Keywords: Molybdenum sulfide, Carbon nanotubes, Electrocatalyst, Hydrogen evolution reaction, Alkaline electrolyte

1. Introduction

The long-term use of fossil fuels has caused environmental pollution and energy shortages, search and design of green renewable conversion with their high energy density and low cost has received increasing attention. Hydrogen, as a clean energy source, has been considered as a promising alternative for traditional fossil fuels in the future due to its high energy density and low cost [1]. Among various hydrogen production technologies, the hydrogen evolution reaction (HER)

* Corresponding author: weiax@gdut.edu.cn

<https://doi.org/10.15251/DJNB.2022.173.799>

from water splitting has the advantages of high purity, simple process, no pollution and so on [2]. However, the hydrogen evolution reaction requires efficient, durable and low-cost catalyst, therefore, the design and preparation of high-efficiency nonprecious metal catalyst for the HER are essential to realizing hydrogen economy and promoting sustainable development in the future.

Two-dimensional (2D) layered transition metal sulfide (TMDs) is bonded through strong covalent bonds within the layers, and is bonded through weak van der Waals forces between the interlayer so that there is strong bonding within the layers and weak interlayer interactions. The unique structure and unusual properties make 2D TMDs becomes highly efficient catalysts for the HER [3-5]. Currently, MoS₂ is the most widely studied 2D TMD as a catalyst for the HER. Both experimental and theoretical investigations have indicated that the HER activity of MoS₂ correlates with the number of its unsaturated active edge sites [6-8]. Nowadays, various synthetic methods were reported to prepare MoS₂ with various morphologies, such as ultrathin flakes [9], nanoflowers [10], thin films [11], nanoplates [12], nanoribbons [13], nanotubes [14], fullerene-like nanoparticles [15] and nanosheet arrays [16]. Li et al. prepared the MoS₂ nanoflowers constructed with nanosheets using a facile hydrothermal method [17]. The MoS₂ nanoflowers ink was prepared by adding MoS₂ nanoflowers powder into ethanol containing nafion. The working electrode for the HER was prepared by spreading the MoS₂ nanoflowers ink onto the surface of glassy carbon. The obtained MoS₂ nanoflowers electrode exhibited the overpotential of 255 mV at current density of 10 mA cm⁻² and a Tafel slope of 77.7 mV dec⁻¹ for the HER. Kong et al. synthesized of MoS₂ films with vertically aligned layers on mirror-polished glassy carbon substrates by a rapid sulfurization of ultrathin Mo films. The MoS₂ thin films with vertically aligned layers maximally expose the edge sites on the surface, and have excellent catalytic activity in the HER [18]. The exchange current density and Tafel slope are 2.2×10⁻⁶ A cm⁻² and 75 mV dec⁻¹, respectively. The exchange current density correlates directly with the density of the exposed edge sites. Xie et al. put forward engineering defect structure on the basal planes of MoS₂ to increase the exposure of active edge sites [19]. They prepared defect-rich MoS₂ nanosheets by designing a reaction with a high concentration of precursors and excess thiourea. The existence of rich defects in the ultrathin MoS₂ nanosheets results in partial cracking of the catalytically inert basal planes, leading to exposure of additional active edge sites. The defect-rich MoS₂ ultrathin nanosheets exhibit excellent HER activity with a small onset overpotential of 120 mV and a small Tafel slope of 50 mV dec⁻¹. Deng et al. developed a synergistic N doping and PO₄³⁻ intercalation strategy to induce phase transformation from 2H-MoS₂ to 1T-MoS₂ with a high conversion of about 41%, leading to superior HER performance with a lower Tafel slope of 42 mV dec⁻¹ and overpotential of 85 mV at current density of 10 mA cm⁻² [20]. From what has been discussed above, the HER activity of the catalyst can be improved not only by increasing numbers of active sites by a phase transition or the introduction of defects and vacancies, but also by improving the conductivity of the catalyst [21, 22].

In this work, a facile hydrothermal method was used to grow MoS₂ nanosheets on a carbon nanotubes (CNTs)/carbon cloth (CC) substrate using a precursor solution of Na₂MoO₄·2H₂O, SC(NH₂)₂, C₂H₂O₄·2H₂O and de-ionized water. Because the poor conductivity of MoS₂ itself significantly limit the overall HER rate, therefore, a CNTs/CC substrate was used as substrate to enhance HER activity of MoS₂ nanosheets. The MoS₂/CNTs/CC catalysts were prepared by changing the oxalic acid concentrations in a precursor solution. The effects of the

oxalic acid concentrations in a precursor solution on the electrocatalytic performance of MoS₂/CNTs/CC catalysts for the HER were studied.

2. Experimental

2.1. Hydrothermal synthesis of MoS₂ nanosheets on a CNTs/CC substrate

MoS₂ nanosheets were synthesized on a carbon nanotubes/carbon cloth (CNTs/CC) by hydrothermal method. The CNTs/CC substrate was produced by Heshi New Materials Co. Ltd. The overall thickness of carbon nanotubes/carbon cloth is 0.2 mm. The loading of carbon nanotubes is 3-4 mg cm⁻², the diameter of carbon nanotubes is 25-50 nm, and the diameter of carbon fiber is 10-25 μm. The conductivity of carbon nanotubes/carbon cloth is 138-150 S cm⁻¹. A typical synthesis process is described as follows: 0.4 mmol Na₂MoO₄·2H₂O, 1.5 mmol SC(NH₂)₂ and 0.225 mmol C₂H₂O₄·2H₂O were dissolved and stirred in 40 ml deionized water as the reaction solution. The reaction precursor was then poured into a Teflon liner with a volume of 60 mL, and then three CNTs/CC substrates (1×2 cm²) were placed diagonally against the inner wall of the Teflon liner. The Teflon liner was loaded into a stainless steel autoclave and heated at 200 °C for 8 h. Thereafter, the autoclave was naturally cooled to room temperature. The MoS₂/CNTs/CC samples were removed and washed with water and ethanol several times, and then the MoS₂/CNTs/CC samples were dried by nitrogen gas. To study the effects of the oxalic acid concentration in a reaction solution on the morphology, crystallographic structure and electrocatalytic performance of MoS₂/CNTs/CC, a series samples were prepared by varying the oxalic acid concentration from 0, 1.875, 3.75 to 5.625 mM. The corresponding samples were marked as samples A1, A2, A3 and A4. The preparation process parameters of various samples are shown in Table 1. The loading mass of MoS₂ nanosheets grown on CNTs/CC was estimated to be 0.425 mg cm⁻².

Table 1. Parameters of preparation process for MoS₂ nanosheets.

Sample No	Na ₂ MoO ₄ mmol	SC(NH ₂) ₂ mmol	C ₂ H ₂ O ₄ ·2H ₂ O mmol	Water ml	Temperature °C	Reaction time h
A1	0.4	1.5	0	40	200	8
A2	0.4	1.5	0.075	40	200	8
A3	0.4	1.5	0.150	40	200	8
A4	0.4	1.5	0.225	40	200	8

2.2. Characterization of the MoS₂ nanosheets/CNTs/CC

The morphology and element distribution map of the MoS₂ nanosheets were observed using scanning electron microscopy (SEM, SU8010, Hitachi) and energy dispersive spectrometer (EDS, SU8010, Hitachi). The crystal structures of the MoS₂ nanosheets were characterized by X-ray diffraction (D/MAX-Ultima, Rigaku), Raman spectroscopy (LabRAM HR Evolution, HORIBA Jobin Yvon) and transmission electron microscopy (TEM, JEM-2100, JEOL). For TEM imaging, sample A1 was dispersed by ultrasound in 5mL anhydrous ethanol for 15 min, then

dropped onto a porous carbon coated 200-mesh copper grid and dried under ambient air at room temperature.

2.3. Electrochemical measurement of MoS₂ nanosheets/CNTs/ CC

All electrochemical measurement was carried out using the electrochemical workstation (CHI760E, Shanghai Chenhua Company). The three-electrode system was employed, where mercury - mercury oxide electrode (Hg/HgO) was used as reference electrode, a graphite rod as pair electrode, and a 1×1 cm² MoS₂/CNTs/CC as working electrode. 1 M KOH (pH 14) was used as an electrolyte. Before the HER test, MoS₂/CNTs/CC electrodes were pretreated via a certain number of Cyclic voltammetry (CV) cycles to activate and stabilize the catalysts. Linear sweep voltammetry (LSV) was performed with scan rate of 5 mV s⁻¹. In LSV test, iR compensation is performed on the data, where *i* is the current density and *R* is the solution resistance. CV was tested in the non-Faraday range of -0.9 to -0.8 V (vs. Hg/HgO) at different scanning speeds ranging from 10 to 50 mV s⁻¹. Electrochemical impedance spectroscopy (EIS) was performed under a potential of -1.058 V (vs. Hg/HgO) in the frequency range from 100 kHz to 0.01 Hz with an AC amplitude of 5 mV. The long-term stability of the MoS₂/CNTs/CC catalysts was characterized at a current density of 10 mA cm⁻² by chronopotentiometry. All potential data are converted to the reversible hydrogen electrode (RHE) according to the Nernst equation:

$$E \text{ vs. (RHE)} = E \text{ vs. (Hg/HgO)} + 0.098 + 0.0591 \times \text{pH} \quad (1)$$

3. Results and discussions

3.1. Characterization of MoS₂ nanosheets/CNTs/CC

Fig.1 shows SEM images of bare CNTs/CC and samples A1, A2, A3, A4, respectively. It can be clearly seen in Fig. 1a that the surface of the carbon cloth is evenly covered with carbon nanotubes. As can be observed from Fig.1b to Fig.1e, the oxalic acid concentration in the precursor solution has a significant effect on the size and morphology of MoS₂ nanosheets. When the oxalic acid concentration is 0 (sample A1) and 1.875 mM (sample A2), many MoS₂ nanosheets gather together perpendicular to the spherical surface and form flower-like nanosheets microspheres, which cover on surface of CNTs/CC substrate. The diameter of MoS₂ nanosheets microspheres is about 0.9 and 0.3 μm for samples A1 and A2, respectively. However, for sample A1, the coverage of MoS₂ nanosheets microspheres on surface of CNTs is poor. For sample A2, the MoS₂ nanosheets microspheres uniformly and densely cover the surface of CNTs/CC substrate. When the oxalic acid concentration is increased 3.750 mM (sample A3), only a small amount of MoS₂ nanosheets microspheres are distributed on the surface of CNTs/CC substrate, while the fine MoS₂ wrap on CNTs. However, when the oxalic acid concentration is further increased to 5.625 mM (sample A4), the fine MoS₂ nanosheets are wrapped on the surface of CNTs as shown in Fig. 1e. The MoS₂ nanosheets microspheres are no longer formed. Fig.1f shows low-magnification SEM image and the corresponding S, Mo and C elemental mapping images (EDX) of sample A4 prepared at the oxalic acid concentration of 5.625 mM. The S and Mo elements are homogeneously distributed throughout the CNTs.

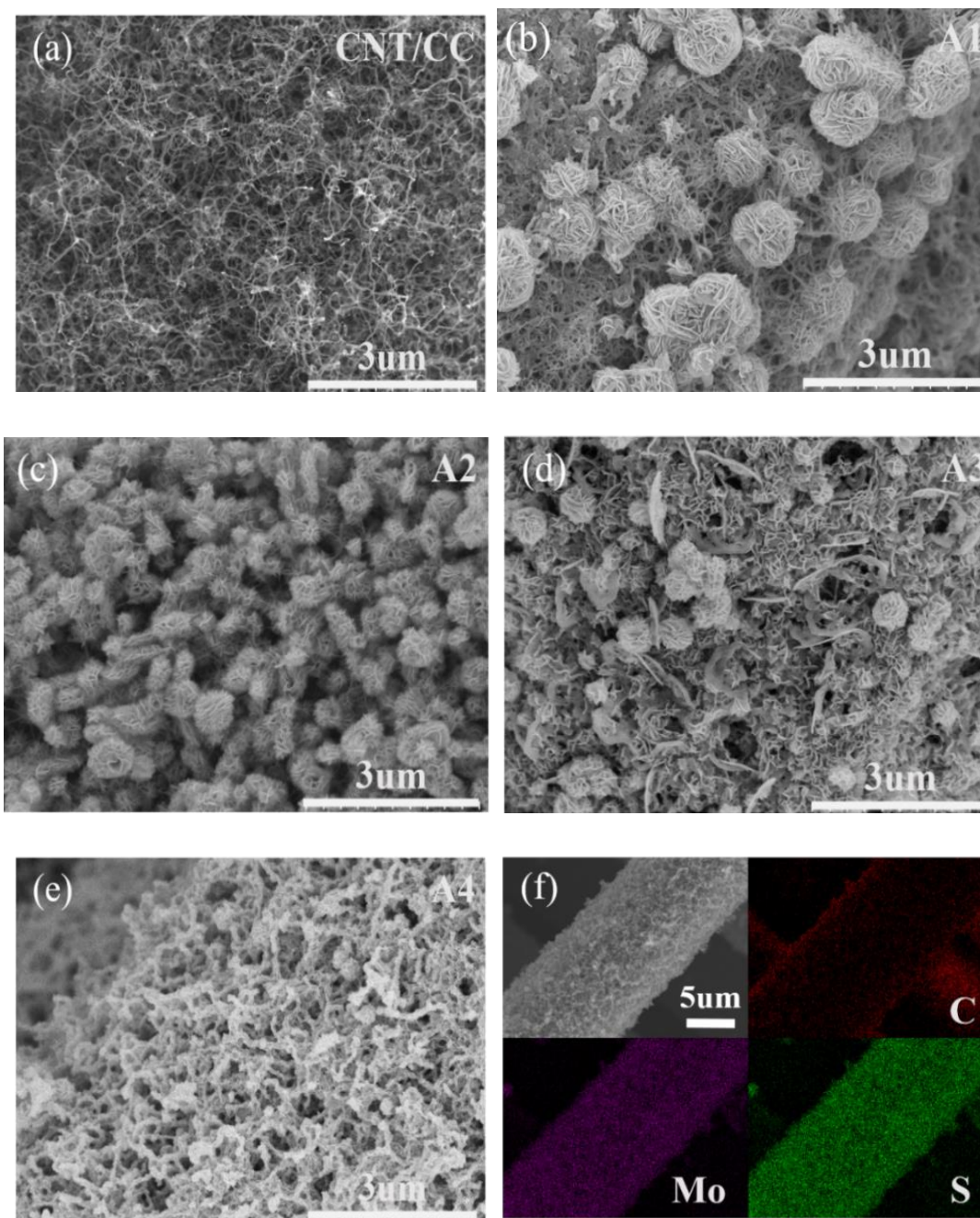


Fig. 1. (a) SEM images of bare CNTs/CC; (b-e) SEM images of samples A1, A2, A3 and A4; (f) Low-magnification SEM image and EDX elemental mapping images of sample A4.

In a precursor solution, $\text{SC}(\text{NH}_2)_2$ is used not only as a S^{2-} ions source, but also as a reducing agent in hydrothermal process. As can be seen from Fig. 1, when there is no oxalic acid in the precursor solution, the flower-like MoS_2 nanosheets microspheres with bigger diameter can be formed (sample A1). The oxalic acid acts also as a reducing agent, which benefits the reduction of Mo^{6+} to Mo^{4+} . The Mo^{4+} then connects with S^{2-} to form MoS_2 . The nucleation rate and reaction rate of MoS_2 will increase with the increasing of oxalic acid concentrations, resulting in the

decreasing of size of MoS₂ nanosheets. When oxalic acid concentration is excessive, only small MoS₂ particles is formed. A detailed reaction process and growth mechanism of MoS₂ nanosheets microspheres were proposed in previous work [23].

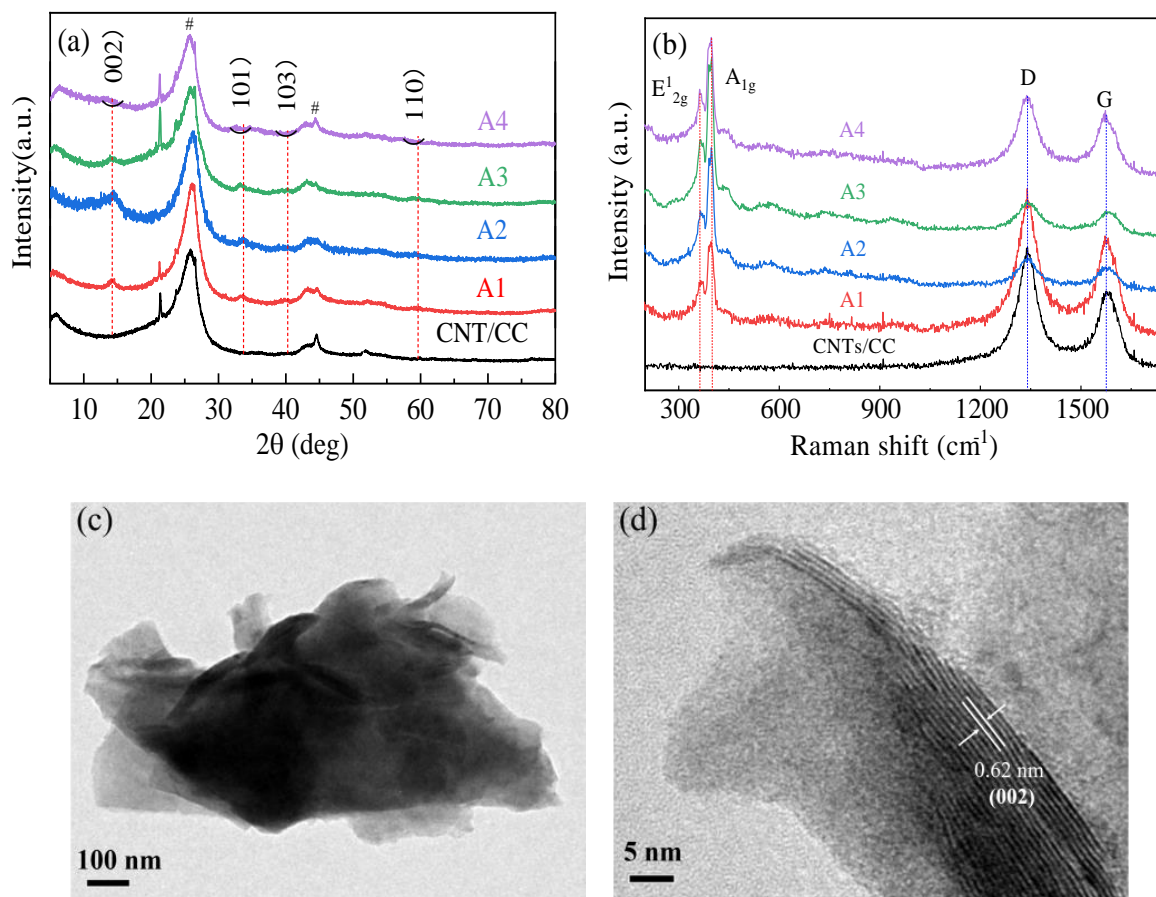


Fig. 2. (a) X-ray diffraction patterns of samples A1, A2, A3, A4 and bare CNTs/CC; (b) Raman spectrum of samples A1, A2, A3, A4 and bare CNTs/CC; (c, d) TEM and HRTEM image of sample A1.

The XRD patterns of bare CNTs/CC and MoS₂/CNTs/CC prepared using different oxalic acid concentration are shown in Fig. 2a. The diffraction peaks (marked by #) at $2\theta=25.6^\circ$ and 43.5° correspond to the (0 0 2) and (1 0 0) crystal planes of carbon cloth substrate [24]. The diffraction peaks of CNTs are also very close to those of carbon cloth [25]. The diffraction peaks at $2\theta=14.4^\circ$, 33.6° , 39.6° and 58.4° are assigned the (0 0 2), (1 0 1), (1 0 3) and (1 1 0) planes of hexagonal phase of MoS₂ (JCPDS No. 37-1492) respectively. The morphology of sample A4 is very different with that of samples A1, A2 and A3, but the diffraction peaks of samples A4 are identical to those of these samples. The Raman spectrum to bare CNTs/CC and the as-prepared MoS₂/CNTs/CC is demonstrated in Fig. 2b. The Raman characteristic peaks at 1345.6 and 1580.8 cm⁻¹ can be ascribed to the D and G bands of the CNTs/CC substrate. I_D/I_G is the strength ratio of peak D to peak G, and the I_D/I_G ratio generally indicates the degree of defect density. There are

vacancies, edge defect, grain boundaries and disordered carbon types in carbon nanotubes. The higher the I_D/I_G ratio is, the greater the degree of defect. The I_D/I_G ratio of CNTs/CC, A1, A2, A3 and A4 is 1.14, 1.10, 1.05, 1.06 and 1.05, respectively, this is because the defects of CNTs participate in the reaction of MoS_2 in the reaction process [26]. Two Raman characteristic peaks located at 368 and 401 cm^{-1} are corresponding to vibration model of in-plane (E_{2g}) and vibration models of out-of-plane (A_{1g}) of hexagonal MoS_2 , respectively. A high-resolution transmission electron microscope (HRTEM) is used to further study the crystal structure of MoS_2 nanosheets. Fig. 2c and Fig. 2d provide TEM and HRTEM images of MoS_2 nanosheets (sample A1). The lattice spacing is 0.62 nm is corresponds to the (0 0 2) interlayer spacing of the hexagonal phase of MoS_2 crystal. The interlayer spacing of 0.62 nm corresponds to the distance between the layers of two-dimensional MoS_2 nanosheets. Each nanosheet is composed of approximately 10–15 layers.

3.2. Electrocatalytic performance of $\text{MoS}_2/\text{CNTs}/\text{CC}$ catalyst in the HER

To study the effect of substrate on HER catalytic activity of MoS_2 nanosheets, MoS_2 nanosheets were grown on CC and CNTs/CC substrates under the same conditions. Fig. 3a shows LSV polarization curves of CC, CNTs/CC, MoS_2/CC and $\text{MoS}_2/\text{CNTs}/\text{CC}$, respectively. The overpotentials of CC, CNTs/CC, MoS_2/CC and $\text{MoS}_2/\text{CNTs}/\text{CC}$ are 508, 223, 199 and 130 mV at a current density of 10 mA cm^{-2} , respectively. The pure CC electrode has poor HER activity. The overpotential of CNTs/CC is 285 mV less than that of CC electrode, the overpotential of $\text{MoS}_2/\text{CNTs}/\text{CC}$ is 69 mV less than that of MoS_2/CC . Therefore, CNTs/CC as a substrate is more advantageous for HER than CC as a substrate. To study the effect of the oxalic acid concentrations in the precursor solution on the electrocatalytic performance of $\text{MoS}_2/\text{CNTs}/\text{CC}$ catalyst for HER, LSV polarization curves of samples A1, A2, A3 and A4 are tested, and the results are shown in Fig. 3b. The overpotentials of samples A1, A2, A3 and A4 are 254, 174, 174 and 130 mV, respectively. The oxalic acid concentration in the precursor solution has an obvious effect on the overpotentials of $\text{MoS}_2/\text{CNTs}/\text{CC}$ catalysts. The overpotentials of $\text{MoS}_2/\text{CNTs}/\text{CC}$ catalysts decrease gradually with the increase of oxalic acid concentration in the precursor solution.

The hydrogen evolution reaction (HER) from water splitting includes two steps. The first step is hydrogen binds to the catalyst (Volmer adsorption). The second step involves the formation and desorption of hydrogen by either the Heyrovsky reaction or Tafel reaction [27, 28]. The Tafel slopes for the Volmer, Heyrovsky and Tafel reaction are 120, 40, and 30 mV dec^{-1} , respectively [27, 29]. Therefore, Tafel slope reflects the HER kinetic process and charge transfer ability of electrocatalysts. To further study the HER dynamics of $\text{MoS}_2/\text{CNTs}/\text{CC}$, Tafel curves of samples are plotted according to the LSV polarization curve in Fig.3b. Tafel curves of samples are shown in Fig.3c. The slope of the linear portion of Tafel curve is defined as Tafel slope. Tafel slopes for samples A1, A2, A3 and A4 are 104.8, 83.6, 80.0 and 45.7 mV dec^{-1} , respectively, indicating a typical Volmer-Heyrovsky route with the Volmer step as the rate-determining step. Tafel slope is inversely proportional to the charge transfer coefficient of the electrocatalysts. Our SEM and Tafel slope analysis results indicate that smaller MoS_2 nanosheets are beneficial for hydrogen adsorption and desorption.

The CV curves of samples were measured at scan rates of 10, 20, 30, 40 and 50 mVs^{-1} , respectively. Fig.3d provides the CV curves of sample A4. From the CV curve, the dependence of the current density difference Δj ($\Delta j = j_a - j_b$, where j_a and j_b denote the current densities in CV curves at a middle potential) on the scan rate can be obtained, as shown in Fig. 3e. The current

density difference Δj and scan rate follows an almost linear relationship, and one-half of its slope is defined as the electrochemical double layer capacitance C_{dl} . The C_{dl} values of samples A1, A2, A3 and A4 are 104.9, 48.9, 61.9 and 123.9 mF cm^{-2} , respectively. The electrochemical surface area (ECSA) of the catalysts can be calculated according to the Randles–Sevcik equation [30, 31]:

$$ECSA = \frac{C_{dl}}{C_s} = \frac{C_{dl}}{40 \mu\text{F cm}^{-2} \text{ per cm}_{ECSA}^{-2}} \quad (2)$$

where C_s is specific capacitance, it is generally in the range of 20~60 $\mu\text{F cm}^{-2}$. C_s value of 40 $\mu\text{F cm}^{-2}$ is used for the calculation of the ECSA [30]. The ECSA values of samples were estimated using C_{dl} and Equation (2), they are 2622.5, 1222.5, 1547.5 and 3097.5 cm^2 for samples A1, A2, A3 and A4, respectively. The larger the ECSA, the more active sites on surface of MoS_2 CNTs/CC catalyst.

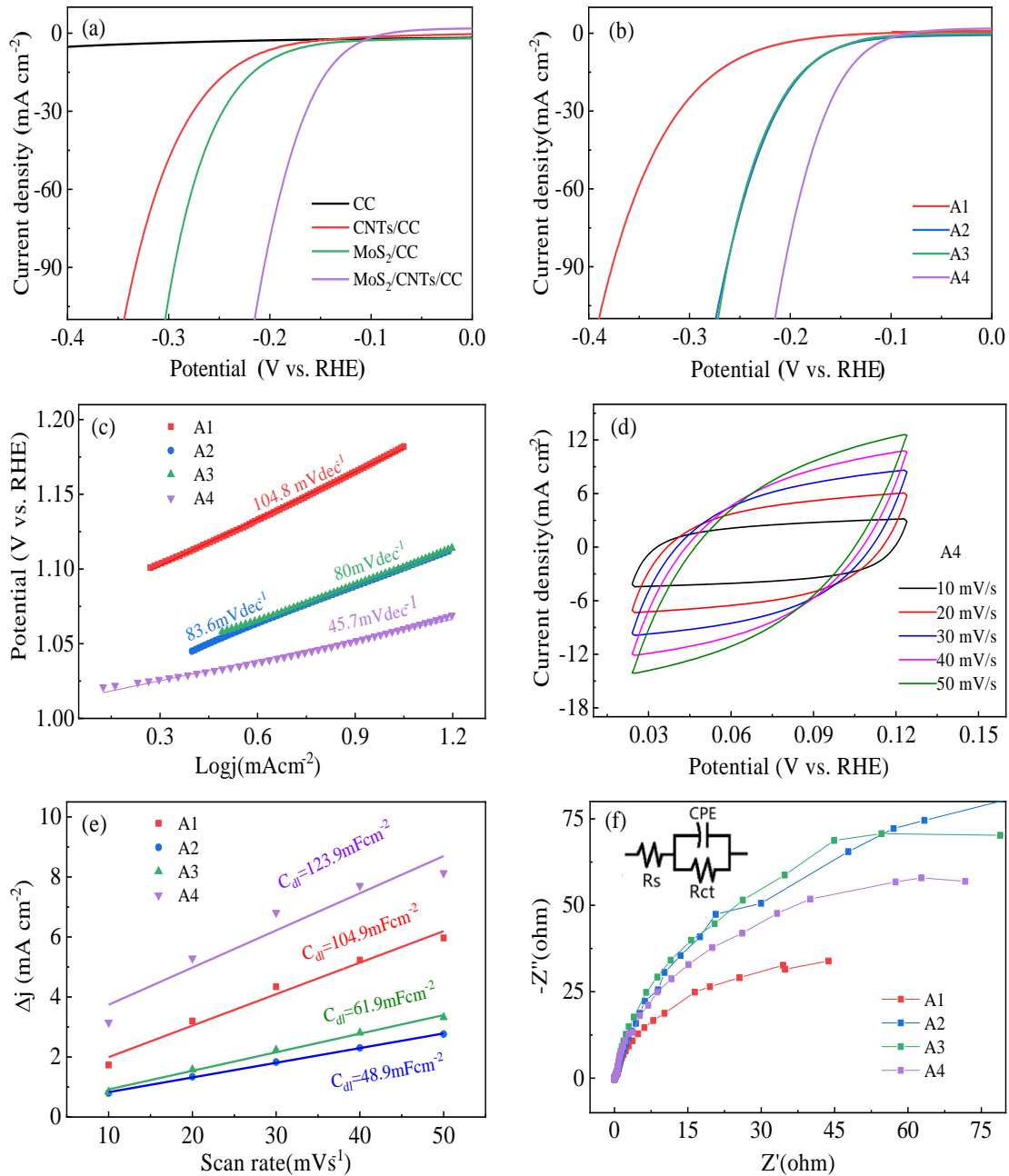
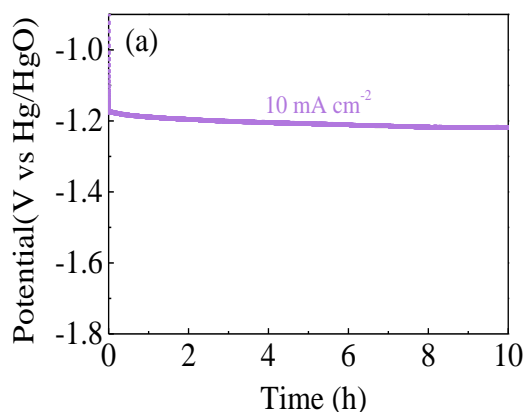


Fig. 3. Electrocatalytic HER properties for samples A1, A2, A3 and A4 in the 1 M KOH electrolyte; (a, b) LSV polarization curves; (c) Tafel plots; (d) C-V curves of sample A4; (e) Dependence of current density with scan rate; (f) Nyquist plots.

Based on the above experimental results, we can conclude that the oxalic acid concentration in the precursor solution plays a key role on the size of MoS₂ nanosheets, it has obvious effect on HER activity of MoS₂ CNTs/CC catalyst. Sample A4 prepared with the oxalic acid concentration of 5.625 mM exhibits an optimal electrocatalytic performance, yielding overpotential of 134 mV at a current density of 10 mA cm⁻², Tafel slope of 45.7 mV dec⁻¹, electrochemical double layer capacitance of 123.9 mF cm⁻² and maximum electrochemical surface area of 3097.5 cm². For sample A4, the surface of the carbon nanotubes is densely packed and uniformly covered by small MoS₂ nanosheets (Fig. 1). Compared with samples A1, A2 and A3, sample A4 not only can provide more abundant catalytic active edge sites, but also can improve the electrical conductivity of catalysts. Therefore, it exhibits an optimal HER activity.

The charge transport capability of catalyst has an important influence on the electrocatalytic performance. Electrochemical impedance spectroscopy (EIS) was employed to analyze the charge transport properties at the MoS₂ catalyst/ Electrolyte interfaces. The Nyquist plots of samples are shown in Fig.3f. The inset in Fig. 3f is equivalent circuit where R_{ct} is the charge transfer resistance at the MoS₂/CNTs/CC electrode and electrolyte interface; C_{PE} is similar to the electrochemical double layer capacitance and R_s is the electrolyte resistance. R_{ct}, C_{PE} and R_s can be obtained by fitting the equivalent circuit to Nyquist plots using ZSimpWIN software. The charge transfer resistance R_{ct} for samples A1, A2, A3 and A4 is 8.0, 212.4, 191.2 and 135.0 Ω, respectively. Compared to samples A2 and A3, sample A4 has a smaller the charge transfer resistance, which indicates that sample A4 has the fastest electron transfer and the fastest HER kinetics in a strong alkaline solution. Although the charge transfer resistance R_{ct} of sample A1 is the smallest, however, this is because the low coverage of MoS₂ on the CNTs surface, and the part of the CNTs is exposed (as observed from Fig.1b), resulting in a small R_{ct}. In addition, the electrolyte resistance R_s is equal to 1.8Ω.



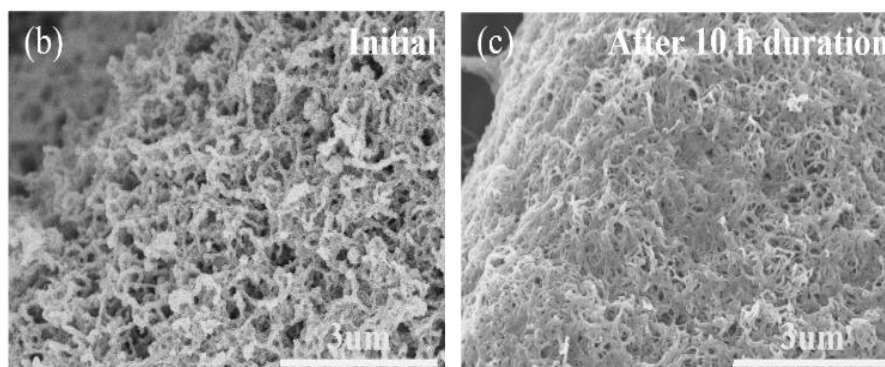


Fig. 4. (a) time-dependent potential (vs. Hg/HgO) curve at the current density of 10 mA cm^{-2} ; (b, c) SEM images for sample A4 before and after the 10 h long-term stability test.

The stability of electrocatalysts is also very important in industrial applications. The long-term stability of samples A4 was carried out using chronopotentiometry test at 10 mA cm^{-2} for 10 h duration. The time dependence of the potential is displayed in Fig. 4a. There is no obvious decay observed for the electrode after duration of 10 h, demonstrating the very high durability of the $\text{MoS}_2/\text{CNTs}/\text{CC}$ catalyst. Furthermore, SEM images of sample A4 at initial and after 10 h stability test are displayed in Fig. 4b and Fig. 4c. The result reveals that the morphology of after duration of 10 h well maintained, further suggesting its excellent structure stability.

4. Conclusion

In summary, the MoS_2 nanosheets were successfully grown on a CNTs/CC substrate by hydrothermal method. The effects of the oxalic acid concentrations on the surface morphology, structure and electrocatalytic performance of $\text{MoS}_2/\text{CNTs}/\text{CC}$ were studied. With increasing the oxalic acid concentration in the precursor solution, the size of the MoS_2 nanosheets gradually decreases and HER activity of $\text{MoS}_2/\text{CNTs}/\text{CC}$ catalyst gradually enhance. The $\text{MoS}_2/\text{CNTs}/\text{CC}$ catalyst prepared with the oxalic acid concentration of 5.625 mM has the optimal HER catalytic performance under 1 M KOH electrolyte, exhibiting an overpotential of 134 mV at current density of 10 mA cm^{-2} , Tafel plots of 45.7 mV dec^{-1} , electrochemical double layer capacitance of 123.9 mF cm^{-2} , electrochemical surface area of 3097.5 cm^2 and charge transfer resistance of 135.0Ω . Meanwhile, it also shows relatively good durability in the continuous HER process. The oxalic acid acts as a reducing agent, which benefits the reduction of Mo^{6+} to Mo^{4+} . The Mo^{4+} then connects with S^{2-} to form MoS_2 . The increasing of the oxalic acid concentrations in the precursor solution results in the decreasing of the size of MoS_2 nanosheets. The smaller size can maximally expose more active edge sites and improve HER catalytic performance.

References

- [1] R. Y. Kannah, S. Kavitha, Preethi, O. P. Karthikeyan, G. Kumar, N. V. Dai-Viet, J. R. Banu, *Bioresour. Technol.* 319, 124175 (2021); <https://doi.org/10.1016/j.biortech.2020.124175>

- [2] A. Arregi, M. Amutio, G. Lopez, J. Bilbao, M. Olazar, *Energy Convers. Manag.* 165, 696 (2018); <https://doi.org/10.1016/j.enconman.2018.03.089>
- [3] J. Joyner, E. F. Oliveira, H. Yamaguchi, K. Kato, S. Vinod, D. S. Galvao, D. Salpekar, S. Roy, U. Martinez, C. S. Tiwary, S. Ozden, P. M. Ajayan, *ACS Appl. Mater. Interfaces* 12, 12629 (2020); <https://doi.org/10.1021/acsami.9b17713>
- [4] R. Wang, J. Han, X. Zhang, B. Song, *J. Mater. Chem. A* 6, 21847 (2018); <https://doi.org/10.1039/C8TA05912H>
- [5] Y. Chen, K. Yang, B. Jiang, J. Li, M. Zeng, L. Fu, *J. Mater. Chem. A* 5, 8187 (2017); <https://doi.org/10.1039/C7TA00816C>
- [6] Z. L. He, W. X. Que, *Appl. Mater. Today* 3, 23 (2016); <https://doi.org/10.1016/j.apmt.2016.02.001>
- [7] Y. Wan, Z. Y. Zhang, X. L. Xu, Z. H. Zhang, P. Li, X. Fang, K. Zhang, K. Yuan, K. H. Liu, G. Z. Ran, Y. Li, Y. Ye, L. Dai, *Nano Energy* 51, 86 (2018); <https://doi.org/10.1016/j.nanoen.2018.02.027>
- [8] T. F. Jaramillo, K. P. Jorgensen, J. Bonde, J. H. Nielsen, S. Horch, I. Chorkendorff, *Science* 317, 100 (2007); <https://doi.org/10.1126/science.1141483>
- [9] Z. P. Lin, Z. P. Wang, S. J. Shen, Y. C. Chen, Z. X. Du, W. Y. Tao, A. J. Xu, X. F. Ye, W. W. Zhong, S. S. Feng, *J. Alloys Compd.* 834, 155217 (2020); <https://doi.org/10.1016/j.jallcom.2020.155217>
- [10] Y. Z. Liu, X. Y. Xu, J. Q. Zhang, H. Y. Zhang, W. J. Tian, X. J. Li, M. O. Tade, H. Q. Sun, S. B. Wang, *Appl. Catal. B* 239, 334 (2018); <https://doi.org/10.1016/j.apcatb.2018.08.028>
- [11] Y. Yin, J. Han, Y. Zhang, X. Zhang, P. Xu, Q. Yuan, L. Samad, X. Wang, Y. Wang, Z. Zhang, *J. Am. Chem. Soc.* 138, 7965 (2016); <https://doi.org/10.1021/jacs.6b03714>
- [12] P. Jia, T. Bu, X. Sun, Y. Liu, J. Liu, Q. Wang, Y. Shui, S. Guo, L. Wang, *Food Chem.* 297, 124969 (2019); <https://doi.org/10.1016/j.foodchem.2019.124969>
- [13] Q. Li, E. Walter, W. V. D. Veer, B. Murray, J. Newberg, E. Bohannan, J. Switzer, J. Hemminger, R. Penner, *J. Phys. Chem. B* 109, 3169 (2005); <https://doi.org/10.1021/jp045032d>
- [14] Y. X. Chen, W. J. Ma, K. F. Cai, X. W. Yang, C. J. Huang, *Electrochim Acta* 246, 615 (2017); <https://doi.org/10.1016/j.electacta.2017.06.102>
- [15] A. Zak, Y. Feldman, V. Alperovich, R. Rosentsveig, R. Tenne, *J. Am. Chem. Soc.* 122, 11108 (2000); <https://doi.org/10.1021/ja002181a>
- [16] D. J. Ko, X. Z. Jin, K. D. Seong, B. Y. Yan, H. Chai, J. M. Kim, M. Hwang, J. Choi, W. Zhang, Y. Z. Piao, *Appl. Catal. B* 248, 357 (2019); <https://doi.org/10.1016/j.apcatb.2019.02.035>
- [17] Z. C. Li, J. J. Ma, Y. Zhou, Z. M. Yin, Y. B. Tang, Y. X. Ma, D. B. Wang, *Electrochimica Acta*, 283, 306 (2018); <https://doi.org/10.1016/j.electacta.2018.06.135>
- [18] D. S. Kong, H. T. Wang, J. J. Cha, M. Pasta, K. J. Koski, J. Yao, Y. Cui, *Nano Letters* 13, 1341 (2013); <https://doi.org/10.1021/nl400258t>
- [19] J. F. Xie, H. Zhang, S. Li, R. X. Wang, X. Sun, M. Zhou, J. F. Zhou, X. Wen D. Lou, Y. Xie, *Advanced Materials* 25, 5807 (2013); <https://doi.org/10.1002/adma.201302685>
- [20] S. J. Deng, M. Luo, C. Z. Ai, Y. Zhang, B. Liu, L. Huang, Z. Jiang, Q. H. Zhang, L. Gu, S. W. Lin, X. L. Wang, L. Yu, J. G. Wen, J. A. Wang, G. X. Pan, X. H. Xia, J. P. Tu, *Angew. Chem. Int.*

- Ed. 58, 16289 (2019); <https://doi.org/10.1002/anie.201909698>
- [21] Q. Zhu, Y. Qu, D. Liu, H. Pan, ACS Appl. Nano Mater. 3, 6270 (2020); <https://doi.org/10.1021/acsnm.0c01331>
- [22] H. Yang, T. Zhang, H. Zhu, M. Zhang, W. Wu, M. L Du, Int. J. Hydrog. Energy 42, 1912 (2016); <https://doi.org/10.1016/j.ijhydene.2016.10.075>
- [23] G. B. Feng, A. X. Wei, Y. Zhao, J. Liu, J Mater Sci: Mater Electro 44, 2852 (2015).
- [24] J. C. Wang, J. J. He, G. O. Odunmbaku, S. Zhao, Q. Z. Gou, G. Han, C. H. Xu, - T. Frauenheim, M. Li, Chem. Eng. J. 414, 128811 (2021); <https://doi.org/10.1016/j.cej.2021.128811>
- [25] C. Lee, S. Ozden, C. S. Tewari, O. K. Park, R. Vajtai, K. Chatterjee, P. M. Ajayan. ChemSusChem 11, 2960 (2018); <https://doi.org/10.1002/cssc.201800982>
- [26] A. K. Thakur, A. B. Deshmukh, R. B. Choudhary, I. Karbhal, M. Majumder, M. V. Shelke Mater. Sci. Eng. B 223, 240 (2017); <https://doi.org/10.1016/j.mseb.2017.05.001>
- [27] R. Chen, Y. Ao, C. Wang, P. Wang, ChemComm 56, 8472 (2020); <https://doi.org/10.1039/D0CC01300E>
- [28] Z. S. Zhuo, J. L. Zhu, A. X. Wei, J. Liu, N. Q. Luo, Y. Zhao, Z. Liu, Int. J. Hydrog. Energy 47, 2293 (2022); <https://doi.org/10.1016/j.ijhydene.2021.10.120>
- [29] J. Luxa, P. Marvan, P. Lazar, Z. Sofer, Nanoscale 11, 14684 (2019); <https://doi.org/10.1039/C9NR03281A>
- [30] Y. W. Liu, J. Li, W. T. Huang, Y. Zhang, M. J. Wang, X. S. Gao, W. Wang, M. L. Jin, Z. P. Hou, G. F. Zhou, Z. Zhang, J. M. Liu, ACS Appl. Mater. Interfaces 12, 33586 (2020); <https://doi.org/10.1021/acsnano.6b04725>
- [31] Y. Y. Chen, Y. Zhang, W. J. Jiang, X. Zhang, Z. H. Dai, L. J. Wan, J. S. Song, ACS Nano 10, 8851 (2016); <https://doi.org/10.1021/acsnano.6b04725>